Journal of Materials Chemistry A

Improved Stability and High Thermoelectric Performance Through Cation Site Doping in n-type La-doped $Mg_3Sb_{1.5}Bi_{0.5}$

Journal:	*Journal of Materials Chemistry A*
Manuscript ID	TA-COM-09-2018-008975
Article Type:	Communication
Date Submitted by the Author:	15-Sep-2018
Complete List of Authors:	Imasato, Kazuki; Northwestern University , Materials Science and Engineering; Wood, Max; Northwestern University, Materials Science and Engineering Kuo, Jimmy; Northwestern University, Snyder, G. Jeffrey; Northwestern University, Materials Science

Journal Name

COMMUNICATION

Improved Stability and High Thermoelectric Performance through Cation Site Doping in n-type La-doped $Mg_3Sb_{1.5}Bi_{0.5}$

Received 00th January 20xx,
Accepted 00th January 20xx

DOI: 10.1039/x0xx00000x

www.rsc.org/

Kazuki Imasato,*[a] Max Wood, [a] Jimmy Jiahong Kuo [a] and G. Jeffrey Snyder *[a]

n-type conduction in the $Mg_3Sb_{1.5}Bi_{0.5}$ system is achieved with La-doping on the cation site with peak zT>1. La-doped samples exhibit much higher doping efficiency and dopability compared to other chalcogen-doped samples. This allows greater tunability in electronic properties. La-doping also significantly improves the thermal stability of n-type $Mg_3Sb_{1.5}Bi_{0.5}$ measured via a long-term Hall carrier concentration measurement.

The n-type Mg_3Sb_2-Mg_3Bi_2 alloy can be an exceptionally efficient thermoelectric material because of its highly degenerate conduction band and extremely low lattice thermal conductivity.[1–4] The crystal structure of Mg_3Sb_2 can be thought of in the context of the $CaAl_2Si_2$ structure (space group P-3m1), which consists of the octahedrally coordinated cation Mg^{2+} layer and a tetrahedrally coordinated anion structure $(Mg_2Sb_2)^{-2}$. Long known to be an adequate p-type material through different optimization routes[5–8] (zT≈0.7), band structure calculations on Mg_3Sb_2 had shown it's n-type properties to be superior.[1,2,9] Attempts to dope the material n-type had failed until recently, when chalcogen (Te, Se, S) doped n-type materials were discovered by different research groups[1–3,10–15] which exhibit the promising zT value of ~1.5 at 750 K when alloyed with 25% Mg_3Bi_2.

Initially attempts to realize n-type conduction had failed due to charge compensating vacancy type defects on the cation site (V_{Mg}^{2-}). Once an appreciation of the importance of these charge compensating defects ad their formation energies were realized,[1,16,17] their carrier concentrations were controlled through a process called phase boundary mapping.[3] In the Mg_3Sb_2 system, there are two distinct thermodynamic states where materials could realistically be synthesized; a Mg-excess state and an Sb-excess state where the Mg_3Sb_2 matrix is in equilibrium with elemental Mg or Sb, respectively. The n-type conduction in Mg_3Sb_2-compounds is only attainable when the materials are synthesized in the Mg-excess state because the atomic chemical potential in the Mg excess state suppresses the formation of cation vacancies.[3,17,18] In these high thermoelectric performance n-type materials, extrinsic dopants provide the conduction electrons as opposed to Mg interstitial atoms[3] – the suppression of cation vacancies should enable soluble donor dopant to produce n-type material.

In addition to controlling the charge compensating defects, previous studies revealed the limits of achievable carrier concentration varied depending on the type of electron donating defect that was chosen. $Mg_3Sb_{1.5}Bi_{0.5}$ n-type materials have been synthesized with chalcogen (S, Se, Te) dopants, with S and Se failing to achieve optimal levels of carrier concentration.[14,15] Additionally chalcogen-doped $Mg_3Sb_{1.5}Bi_{0.5}$ suffers from high temperature stability issues, which can be observed as a hysteresis or degradation of n-type carrier concentration with multiple thermal cycles from testing.[1,2,14,15,19] Finally, chalcogen doped samples have a relatively low doping efficiency with Te doped samples reaching a carrier concentration of only approximately 40% of the nominal dopant concentration (expecting $1e^-$ per Te atom) in an optimally doped sample.

Substituting the Group 2 Mg atom with Group 3 elements is a plausible way to dope this alloy by donating one electron per each dopant atom providing the necessary charge carrier concentration and are predicted to be stable.[20] Doping the Mg site might have a more pronounced effect on intrinsic electrical properties than doping the Sb site since the characteristics of the conduction band largely originates from Mg orbitals.[2,9,21] In this study, we have investigated the effect of La-doping for the thermoelectric properties. Based on first-principle calculations, [20] La was predicted to be a more effective dopant for the cation site to control the carrier concentration of n-type $Mg_3Sb_{1.5}Bi_{0.5}$ compared to the chalcogen dopants.

The loss of Mg in n-type $Mg_3Sb_{1.5}Bi_{0.5}$ is a significant issue in this system that needs to be managed (coatings, insulation or cover gas) for practical applications. Experimentally previous studies observed that it is difficult to sustain degenerate n-type carrier behavior at high temperature (>450 C) in chalcogen doped samples.[1,2,14,15] We suspect the cause of this is due to different vapor pressures and reactivity's of the magnesium compared to the pnictide atoms leading to an overall loss of Mg over extended use. As stated earlier the thermodynamic state (whether Mg-excess or Sb-excess) of Mg_3Sb_2 type compounds dramatically effects their defect formation energies and therefore the type and concentration of available charge carriers.

[a] Department of Materials Science and Engineering, Northwestern University, Evanston, IL 60208, USA.

Electronic Supplementary Information (ESI) available: [details of any supplementary information available should be included here]. See DOI: 10.1039/x0xx00000x

Table 1. Hall carrier concentration at 300K compared to the ideally doped samples' carrier concentrations.

$Mg_{3.05}Sb_{1.5}Bi_{.05}X_x$	Hall Carrier Concentration (10^{19}/cm^3)	Ideal Doping Carrier concentration (10^{19}/cm^3)	Doping Efficiency
$X_x = La_{0.005}$	2.91	3.30	88%
$X_x = La_{0.01}$	5.67	6.60	86%
$X_x = La_{0.03}$	6.59	19.8	33%
$X_x = Te_{0.01}$	3.07	6.60	46%

In addition to adjusting the carrier concentration, La substitution for the Mg site might have substantial effect on the high temperature thermal stability of the $Mg_3Sb_{1.5}Bi_{0.5}$ alloy. A small amount of La substitution for Yb in $Yb_{14}MnSb_{11}$ was shown to increase the melting point and reduce the material's overall sublimation rate by changing the bonding character to be more ionic.[22]

We successfully synthesized n-type $Mg_3Sb_{1.5}Bi_{0.5}$ with La-doping and quantitatively evaluate the thermoelectric properties of the material. La-doping is effective not only at realizing n-type conduction but also shows higher doping efficiency for n-type $Mg_3Sb_{1.5}Bi_{0.5}$ compared to chalcogen dopants. Furthermore, an improved thermal stability in the La-doped samples was observed with less change in carrier concentration when placed in a dynamic vacuum at elevated temperature.

La-doping in the Mg_3Sb_2-Mg_3Bi_2 alloy system realizes n-type conduction, with the carrier concentration of this material ranging from ~2.0*10^{19} (1/cm^3) to ~6*10^{19} (1/cm^3) by changing the nominal La concentration (**Figure 1**). Compared to other chalcogen doping, the doping efficiency is higher in cation-doped material which is consistent with the calculation of the defect formation energy.[20] This is plainly seen comparing samples with the same nominal concentration of dopant, with La=0.01 realizing n_H=~5.5*10^{19} (1/cm^3) and Te = 0.01 realizing n_H=~3*10^{19} (1/cm^3) (**Figure SI**). The nominal doping efficiency was calculated by taking the ratio of the Hall carrier concentration to the carrier concentration one would assume if all of the dopant atoms were to donate 1 electron as charge carrier (**Table 1**). The ideally doped carrier concentration was estimated by taking the nominal number of dopant atoms divided by the volume of the compound. We see that La has doping efficiency is roughly double that of Te at similar compositions as shown in **Table 1**. At high levels of La, the doping efficiency begins to decrease hinting that a solubility limit may have been reached. This increase offered by cation doping opens the door for better tuning of electronic properties and potentially reduces impurity phases that would have formed from the excess dopant.

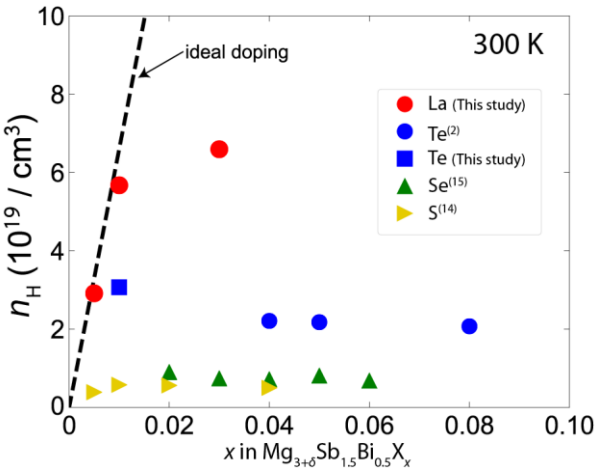

Figure 1. The doping efficiency of $Mg_{3+\delta}Sb_{1.5}Bi_{0.5}$ with La and Chalcogen dopants (Te,[2] Se,[15] S[14]) at 300 K compared to ideal doping (dotted line) calculated based on nominal composition by assuming every dopant donates a carrier. La shows higher doping efficiency compared to chalcogen dopants. Excess Mg (δ) is added to ensure the n-type conduction.

The thermoelectric figure-of-merit zT=1.0 at 600 K is achieved in the La-doped n-type $Mg_3Sb_{1.5}Bi_{0.5}$. Transport properties (**Figure 2**) of $La_xMg_{3.05}Sb_{1.5}Bi_{0.5}$ (x=0.005-0.03) exhibit large values of thermopower showing the typical behavior of degenerate semiconductors. The change in Seebeck coefficient and electrical conductivity is consistent with the change in carrier concentration. The thermally-activated conductivity between 300-500 K can be attributed to the high resistive grain boundary region.[23,24] The different scattering mechanisms cannot mathematically explain the drastic crossover of conductivity from the trend of $T^{1.5}$ to $T^{-1.5}$ within 300-600 K. (See SI of ref. 23) Improved low temperature conductivity in x=0.03 suggests La doping affects both the bulk Fermi level and the grain boundary chemistry.[23] Among our samples with different La content, the sample with La content x=0.05 gives the highest thermoelectric performance with zT=1.0 at 600 K. (**Figure 2**)

A material's figure of merit (zT) is strongly dependent on its carrier concentration as its conductivity, Seebeck coefficient, and electronic portion to thermal conductivity are all functions of Fermi level. Therefore, the dimensionless materials quality factor B was introduced as a fundamental material property not dependent of Fermi level or carrier concentration.[25,26] The material's quality factor B is defined by following equation.[25,26]

$$B = \left(\frac{k_B}{e}\right)^2 \frac{e(2m_e k_B T)^{3/2}}{3\pi^2\hbar^3} \frac{\mu_W}{\kappa_L} T \qquad (1)$$

In this regime, we can evaluate the electrical property and the thermal property separately as the weighted mobility μ_W and lattice thermal conductivity κ_L.

Weighted mobility for each sample is calculated from experimental thermopower and electrical conductivity.[26,27] The temperature dependency of the calculated weighted mobilities for La-doped (La content x=0.005, 0.01, 0.03) and Te doped (Te content 0.01) samples are shown in **Figure 3a**. From this study it appears La doping decreases the intrinsic mobility compared to Te doping. **Figure 3b**, shows a Pisarenko plot (Seebeck coefficient vs Hall carrier concentration) at 300K in which a single parabolic band mass of 1.2m_e agrees well with both Te doped and La doped samples. This

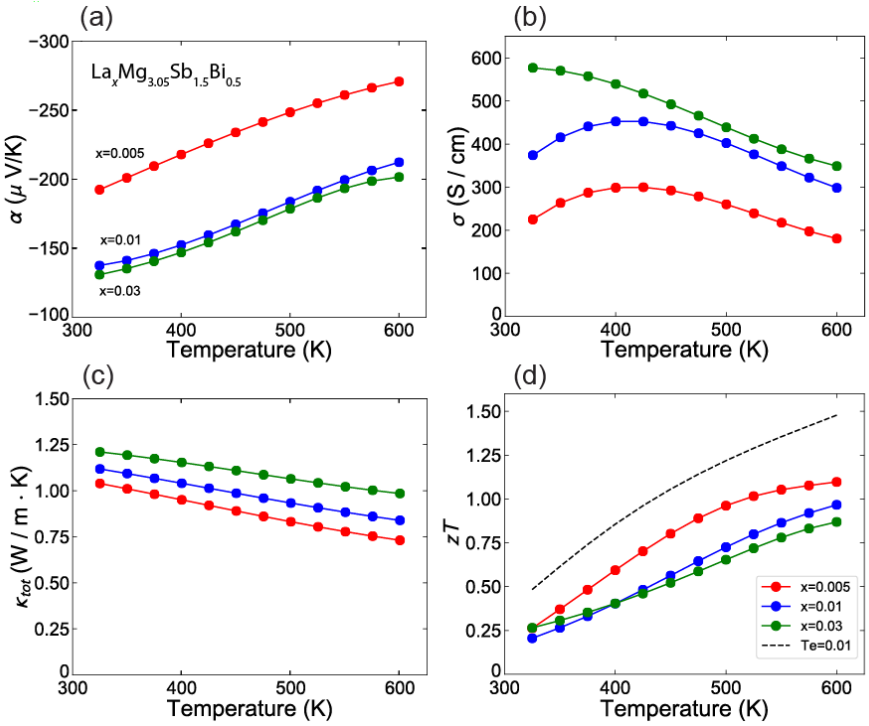

Figure 2 Transport properties of $LaxMg_{3.05}Sb_{1.5}Bi_{0.5}$ (x =0.005-0.03) as a function of temperature: (a) Seebeck coefficient α; (b) electrical conductivity σ; (c) Total thermal conductivity κ_{tot}; (d) Figure-of-merit $zT = \frac{\alpha^2\sigma}{\kappa}T$. The change in transport properties is consistent with carrier concentration change.

indicates that, at least at room temperature, the band structure of the conduction band is not significantly changed by doping with La instead of Te.

To evaluate the change in thermal properties with La-doping, the lattice thermal conductivity $\kappa_L = \kappa_{tot} - \kappa_e$ was obtained by calculating κ_e from Wiedeman-Frantz law, $\kappa_e = LT/\rho$, where L is Lorentz number. Assuming acoustic phonon scattering and a single parabolic band model, the Lorentz number was determined by the experimental Seebeck coefficient.[27] It is noted that the electrical contribution to thermal conductivity can be estimated using bulk Lorenz number as Fermi level calculated from Seebeck coefficient is reflecting mainly the bulk properties. In this method, all the inhomogeneous factor introduced by grain boundary scattering can be approximated to the first order by the conductivity. The calculated lattice thermal conductivity of different La content (x=0.005, 0.01, 0.03) and Te content 0.01 sample are shown in **Figure 3c**. Although we can expect some reduction in lattice thermal conductivity by alloying with heavier elements,[28–31] we do not observe a significant difference in the lattice thermal conductivities between the La and Te-doped samples. This is likely because the amount of dopant is too small to meaningfully change the phonon scattering. The x=0.03 sample possesses slightly higher lattice thermal conductivity compared to other samples which might be attributed to the existence of impurity phase that have higher thermal conductivity with relatively large amount of La as reported in a previous report with different amount of excess Mg.[13] Although this is implied in the decrease in doping efficiency, we could not find any impurity phase in XRD (see Figure SII) since the nominal amount of La is too small to detect.

The quality factor of this material is calculated to be 0.45 at 600 K, which predicts a zT=~1.1 when the material is optimized in terms of carrier concentration. This predicted zT is almost the same value of our best sample (La content x = 0.005) seen in the predicted value of zT depending on carrier concentration plot (**Figure 3d**), which shows this sample carrier concentration is effectively optimized. The quality factor of the La-doped sample is smaller than Te-doped sample, which is due to its smaller weighted mobility. Some of this decrease in mobility is likely attributed to the perturbation of the periodic potential at the conduction band due to the cation site doping by La[21] but could also related to impurity phases that vary with processing conditions.

We have conducted Hall measurements under dynamic vacuum for both a Te-doped and La-doped sample for 72 hours under identical conditions. The goal of this was to see the change Hall-carrier concentration as a function of time at the elevated temperature of 450C, the results of which are seen in (**Figure 4**). Both samples exhibit a linear decrease followed by an exponential decrease (in log y scale) in Hall-carrier concentration. The Te-doped sample only exhibits a linear decrease in Hall-carrier concentration for 1 hour and then exponentially decreases such that within 20 hours the carrier concentration of the Te sample decreased by more than 65% and reaches below n_H = 1*10^{19} (1/cm^3). The La-doped sample shows slow linear decrease for approximately 25 hours, then begins an exponential type decay. The decrease in this linear region is only about 17% which is much lower than decrease of 65% in Te sample. Additionally, over the whole period of measurement the La doped sample loses 62% of its carriers compared to 80% in the Te doped sample. Finally, we would like to note this material has an optimized carrier concentration in the 2-5x10^{19} (1/cm^3) range (figure 3D). At the end of the measurement the La doped sample had a carrier concentration of 1.9x10^{19} (1/cm^3) whereas the Te doped sample had a carrier concentration of 7.2x10^{18} (1/cm^3).

The exponential change in carrier concentration over time at elevated temperatures in these samples is likely related to the Mg

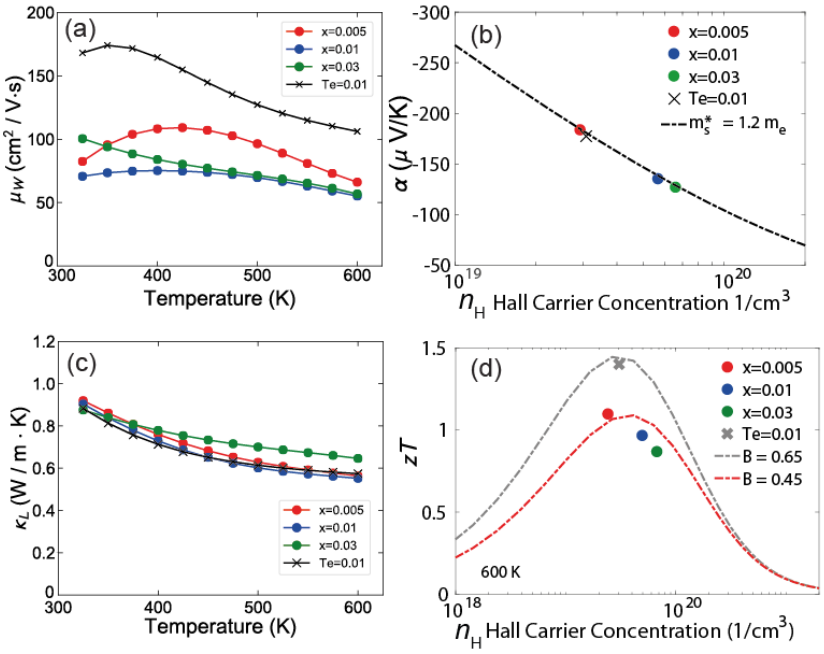

Figure 3 (a) Weighted mobility, (b) Pisarenko plot at 300 K, (c) lattice thermal conductivity and (d) *zT* vs Hall carrier concentration plots at 600 K for $La_xMg_{3.05}Sb_{1.5}Bi_{0.5}$ (*x* =0.005-0.03) and $Mg_{3.05}Sb_{1.5}Bi_{0.5}Te_{0.01}$.

content present in the samples. In dynamic vacuum the excess Mg needed to suppress the formation of electron compensating Mg vacancies[3] slowly decreases due a net loss of Mg. During the regime where there is a slow, linear decrease in Hall-carrier concentration the dopant itself may also be evaporating or its doping efficiency decreasing. However when the Mg evaporation causes the sample to reach the nominal composition where the thermodynamic state is no longer Mg-excess a dramatic change in carrier concentration will occur. Starting at the surface the material will become p-type leading the exponential drop in Hall carrier concentration.

We suspect that cation doping changes the defect energetics in the sample in such a way that it suppresses the net loss of Mg which results in the improvement of thermal stability at high temperature as also reported in 14-1-11 system.[22] Therefore, we can conclude that the La-doping significantly improves the thermal stability of n-type $Mg_{3.05}Sb_{1.5}Bi_{0.5}$, thus, cation-doping can be more realistic strategy to put this material into practice as a thermoelectric generator such as waste heat recovery technology and deep space power generation. Also, we would like to note that the improved thermal stability might also allow the hot pressing of this material at higher temperature. Larger grain size with higher pressing temperature is a useful method to get better electrical performance especially for low temperature by reducing grain boundary resistance.[23,24]

In conclusion, cation-site doping using La for n-type $Mg_{3.05}Sb_{1.5}Bi_{0.5}$ shows higher doping efficiency than anion-site chalcogen doping. Optimized *zT* >1.0 at 600 K was achieved with La content *x*=0.005 in $La_xMg_{3.05}Sb_{1.5}Bi_{0.5}$. Enhanced thermal stability of n-type $Mg_{3.05}Sb_{1.5}Bi_{0.5}$ is observed by La doping. In a long term measurement at the elevated temperature of 450C, degenerate n-type conduction in the La doped sample lasts far longer than in the Te doped sample. While the intrinsic mobility appears to be lower in La-doped samples compared to anion-doped samples, the higher processing temperatures enabled by the enhanced thermal stability may enable future improvements in mobility using optimized processing conditions.

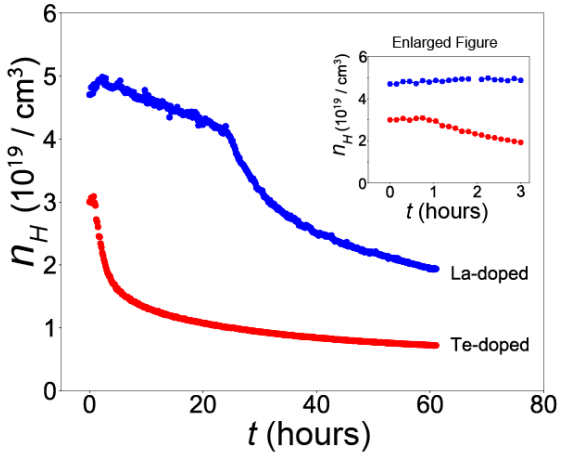

Figure 4 Time dependency of Hall carrier concentration of La-doped sample ($La_{0.01}Mg_{3.05}Sb_{1.5}Bi_{0.5}$) and Te-doped sample ($Mg_{3.05}Sb_{1.5}Bi_{0.5}Te_{0.01}$) measured in a dynamic vacuum that removes Mg vapor.

Experimental Section

$La_xMg_{3.05}Sb_{1.5}Bi_{0.5}$ was synthesized with different values of nominal La (*x* =0.005-0.3). In addition to these samples one sample with Te doping was also synthesized using the same procedure with a

composition of $Mg_{3.05}Sb_{1.5}Bi_{0.5}Te_{0.01}$. We sealed Magnesium turnings (99.98 %, Alfa Aesar), antimony shots (99.9999 %, 5N Plus), bismuth granules (99.999%, 5N Plus), Lanthanum lumps (99.999 %, Alfa Aesar), and Te shot (99.999 %, 5N Plus) into stainless-steel vials according to the nominal composition under the argon-filled glove box. Elements were mechanically alloyed by high energy-ball milling with a high-energy mill (SPEX 8000D) for two hours. The processed powder was loaded into the graphite die and pressed by the induction heating rapid hot press for 20 minutes at 1073 K and 45 MPa under argon gas flow.[32] The Seebeck coefficient of each sample was measured with Chromel-Nb thermocouples in a two-probe configuration under dynamic high vacuum.[33] The Hall coefficient and electric resistivity was measured simultaneously using a 4-point probe Van der Pauw technique with a 2 T magnetic field under dynamic high vacuum. Thermal diffusivity D was measured by using the flash method with a Netzsch LFA 457 under a flowing argon atmosphere. The thermal conductivity κ was calculated by $\kappa = D \times C_p \times d$, where d is density and C_p is heat capacity. (see SI for C_p data) The thermal stability of the materials was measured via the change in the Hall carrier concentration over an extended time at an elevated temperature. With the same set up as the above-mentioned Hall system, we measured Hall coefficient and resistivity for 72 hours for both $La_{0.01}Mg_{3.05}Sb_{1.5}Bi_{0.5}$ and $Mg_{3.05}Sb_{1.5}Bi_{0.5}Te_{0.01}$ under dynamic vacuum at a constant temperature ~450K. Great care was taken to make sure as many experimental details remained identical for both samples such as measuring them at the same time and polishing them to identical thicknesses of 1 mm. We should note that the Hall stage in our set up is made of alumina, which can potentially react with Mg at elevated temperatures.

Acknowledgements

This work was supported by the NASA Science Mission Directorate's Radioisotope Power Systems Thermoelectric Technology Development and the Solid-State Solar- Thermal Energy Conversion Center (S3TEC), an Energy Frontier Research Center funded by the U.S. Department of Energy, Office of Science, Basic Energy Sciences under Award # DE-SC0001299. IMSERC X-ray Facility at Northwestern University is support from the Soft and Hybrid Nanotechnology Experimental (SHyNE) Resource (NSF ECCS-1542205); the State of Illinois and International Institute for Nanotechnology (IIN).

Conflicts of interest

There are no conflicts to declare.

References

1 H. Tamaki, H. K. Sato and T. Kanno, *Adv. Mater.*, 2016, **28**, 10182–10187.

2 J. Zhang, L. Song, S. H. Pedersen, H. Yin, L. T. Hung and B. B. Iversen, *Nat. Commun.*, 2017, **8**, 13901.

3 S. Ohno, K. Imasato, S. Anand, H. Tamaki, S. D. Kang, P. Gorai, H. K. Sato, E. S. Toberer, T. Kanno and G. J. Snyder, *Joule*, 2018, **2**, 141–154.

4 W. Peng, G. Petretto, G.-M. Rignanese, G. Hautier and A. Zevalkink, *Joule*, 2018, **in press**, DOI:10.1016/j.joule.2018.06.014.

5 V. Ponnambalam and D. T. Morelli, *J. Electron. Mater.*, 2013, **42**, 1307–1312.

6 H. X. Xin and X. Y. Qin, *J. Phys. D Appl. Phys.*, 2006, **39**, 5331–5337.

7 S. H. Kim, C. M. Kim, Y.-K. Hong, K. I. Sim, J. H. Kim, T. Onimaru, T. Takabatake and M.-H. Jung, *Mater. Res. Express*, 2015, **2**, 055903.

8 C. L. Condron, S. M. Kauzlarich, F. Gascoin and G. J. Snyder, *J. Solid State Chem.*, 2006, **179**, 2252–2257.

9 J. Li, S. ZHENG, T. Fang, L. Yue, S. Zhang and G. Lu, *Phys. Chem. Chem. Phys.*, 2018, **20**, 7686–7693.

10 J. Shuai, J. Mao, S. Song, Q. Zhu, J. Sun, Y. Wang, R. He, J. Zhou, G. Chen, D. J. Singh, Z. Ren, C. W. Chu, G. Chen and Z. Ren, *Energy Environ. Sci.*, 2017, **10**, 799–807.

11 J. Shuai, J. Mao, S. Song, Q. Zhang, G. Chen and Z. Ren, *Mater. Today Phys.*, 2017, **1**, 74–95.

12 K. Imasato, S. D. Kang, S. Ohno and G. J. Snyder, *Mater. Horizons*, 2018, **5**, 59–64.

13 K. Imasato, S. Ohno, S. D. Kang and G. J. Snyder, *APL Mater.*, 2018, **6**, 016106.

14 J. Zhang, L. Song, K. A. Borup, M. R. V. Jørgensen and B. B. Iversen, *Adv. Energy Mater.*, 2018, 1702776.

15 J. Zhang, L. Song, A. Mamakhel, M. R. V. Jørgensen and B. B. Iversen, *Chem. Mater.*, 2017, **29**, 5371–5383.

16 J. Mao, Y. Wu, S. Song, Q. Zhu, J. Shuai, Z. Liu, Y. Pei and Z. Ren, *ACS Energy Lett.*, 2017, **2**, 2245–2250.

17 S. Ohno, U. Aydemir, M. Amsler, J. H. Pöhls, S. Chanakian, A. Zevalkink, M. A. White, S. K. Bux, C. Wolverton and G. J. Snyder, *Adv. Funct. Mater.*, 2017, **27**, 1606361.

18 J. Shuai, B. Ge, J. Mao, S. Song, Y. Wang and Z. Ren, *J. Am. Chem. Soc.*, 2018, **140**, 1910–1915.

19 L. R. Jørgensen, J. Zhang, C. Zeuthen and B. B. Iversen, *J. Mater. Chem. A*, 2018, **in press**, DOI:10.1039/c8ta06544f.

20 P. Gorai, B. R. Ortiz, E. S. Toberer and V. Stevanović, *J. Mater. Chem. A*, 2018, **6**, 13806–13815.

21 H. Wang, X. Cao, Y. Takagiwa and G. J. Snyder, *Mater. Horizons*, 2015, **2**, 323–329.

22 I. G. Vasilyeva, R. E. Nikolaev, M. N. Abdusaljamova and S. M. Kauzlarich, *J. Mater. Chem. C*, 2016, **4**, 3342–3348.

23 J. J. Kuo, S. D. Kang, K. Imasato, H. Tamaki, S. Ohno, T. Kanno and G. J. Snyder, *Energy Environ. Sci.*, 2018, **11**, 429–434.

24 T. Kanno, H. Tamaki, H. K. Sato, S. D. Kang, S. Ohno, K. Imasato, J. J. Kuo, G. J. Snyder and Y. Miyazaki, *Appl. Phys. Lett.*, 2018, **112**, 033903.

25 R. P. Chasmar and R. Stratton, *J. Electron. Control*, 1959, **7**, 52–72.

26 S. Dongmin Kang and G. Jeffrey Snyder, *Nat. Mater.*, 2016, **16**, 252–257.

27 A. F. May and G. J. Snyder, in *Materials, Preparation, and Characterization in Thermoelectrics*, ed. D. M. Rowe, CRC Press, 2012, pp. 1–18.

28 F. Gascoin, S. Ottensmann, D. Stark, S. M. Haïle and G. J. Snyder, *Adv. Funct. Mater.*, 2005, **15**, 1860–1864.

29 X.Shi, Y. Pei and D. T. Morelli, *Appl. Phys. Lett.*, 2009, **94**, 122112.

30 H. Wang, A. D. Lalonde, Y. Pei and G. J. Snyder, *Adv. Funct. Mater.*, 2013, **23**, 1586–1596.

31 J. Yang, G. P. Meisner and L. Chen, *Appl. Phys. Lett.*, 2004, **85**, 1140–1142.

32 A. D. LaLonde, T. Ikeda and G. J. Snyder, *Rev. Sci. Instrum.*, 2011, **82**, 025104.
33 S. Iwanaga, E. S. Toberer, A. Lalonde and G. J. Snyder, *Rev. Sci. Instrum.*, 2011, **82**, 063905.

The table of contents

Improved Stability and High Thermoelectric Performance through Cation Site Doping in n-type La-doped $Mg_3Sb_{1.5}Bi_{0.5}$

*Kazuki Imasato,[1] Max Wood,[1], Jimmy Jiahong Kuo[1], G. Jeffrey Snyder[1]**

n-type conduction in $Mg_3Sb_{1.5}Bi_{0.5}$ system is achieved with La-doping on cation site with peak zT>1.